AGU PUBLICATIONS

JGR

Journal of Geophysical Research: Solid Earth

RESEARCH ARTICLE

10.1002/2015JB012038

Key Points:
- Anomalously large *PKiKP/PcP* amplitude ratios observed globally
- No hemispherical structure on the inner core boundary
- Regional variation in *PKiKP-PcP* differential travel time residuals

Supporting Information:
- Text S1, Tables S1 and S2, and Figures S1–S3

Correspondence to:
L. Waszek,
lw313@cam.ac.uk

Citation:
Waszek, L., and A. Deuss (2015), Anomalously strong observations of *PKiKP/PcP* amplitude ratios on a global scale, *J. Geophys. Res. Solid Earth*, *120*, 5175–5190, doi:10.1002/2015JB012038.

Received 18 MAR 2015
Accepted 30 JUN 2015
Accepted article online 2 JUL 2015
Published online 21 JUL 2015

Anomalously strong observations of *PKiKP/PcP* amplitude ratios on a global scale

Lauren Waszek[1] and Arwen Deuss[2]

[1]Bullard Laboratories, University of Cambridge, Cambridge, UK, [2]Department of Earth Sciences, Utrecht University, Utrecht, Netherlands

Abstract The inner core boundary marks the phase transition between the solid inner core and the fluid outer core. As the site of inner core solidification, the boundary provides insight into the processes generating the seismic structures of the inner core. In particular, it may hold the key to understanding the previously observed hemispherical asymmetry in inner core seismic velocity, anisotropy, and attenuation. Here we use a large *PKiKP-PcP* amplitude ratio and travel time residual data set to investigate velocity and density contrast properties near the inner core boundary. Although hemispherical structure at the boundary has been proposed by previous inner core studies, we find no evidence for hemispheres in the amplitude ratios or travel time residuals. In addition, we find that the amplitude ratios are much larger than can be explained by variations in density contrast at the inner core boundary or core-mantle boundary. This indicates that *PKiKP* is primarily observed when it is anomalously large, due to focusing along its raypath. Using data in which *PKiKP* is not detected above the noise level, we calculate an upper estimate for the inner core boundary (ICB) density contrast of 1.2 kg m^{-3}. The travel time residuals display large regional variations, which differ on long and short length scales. These regions may be explained by large-scale velocity variations in the *F* layer just above the inner core boundary, and/or small-scale topography of varying magnitude on the ICB, which also causes the large amplitudes. Such differences could arise from localized freezing and melting of the inner core.

1. Introduction

The Earth's inner core gradually grows over time, as material from the liquid outer core solidifies onto its surface. The inner core boundary (ICB) marks the point of solidification of the inner core, where some of the seismic properties are frozen into the material of the inner core. Hence, studying the nature of the ICB has important consequences for understanding the structural variations in the inner core. Inner core studies have revealed increasingly complicated seismic structures, including velocity anisotropy [*Poupinet et al.*, 1983; *Morelli et al.*, 1986; *Woodhouse et al.*, 1986; *Deuss et al.*, 2010; *Irving and Deuss*, 2011], hemispherical variations in compressional velocity [*Tanaka and Hamaguchi*, 1997; *Niu and Wen*, 2001; *Cao and Romanowicz*, 2004b; *Oreshin and Vinnik*, 2004; *Waszek et al.*, 2011], and corresponding properties in attenuation [*Wen and Niu*, 2002; *Cao and Romanowicz*, 2004b; *Souriau*, 2009; *Waszek and Deuss*, 2013]. However, the cause of these features is a topic of debate, and current geodynamic models cannot fully explain the seismic observations. It is currently unclear whether the velocity and attenuation variations continue up to the ICB. This is crucial for determining whether the mechanisms such as freezing and melting of the ICB are regional or hemispherical.

The quasi hemispherical difference in seismic properties has been observed down to almost the center of the inner core [*Oreshin and Vinnik*, 2004; *Lythgoe et al.*, 2014]. The east hemisphere has higher seismic velocity and stronger attenuation than the west hemisphere. Deeper regions in parts of the west hemisphere display depth-dependent anisotropy aligned to the Earth's rotation axis, whereby rays traveling in a polar direction travel faster than equatorial paths [*Irving and Deuss*, 2011]. The upper 60–100 km of the inner core is nearly isotropic in both hemispheres [*Shearer*, 1994; *Song and Helmberger*, 1998; *Waszek and Deuss*, 2011]. The hemispherical difference in isotropic velocity has been observed from a depth of ~15 km below the ICB [*Waszek et al.*, 2011]; however, it is unclear whether it extends up to the ICB.

There are currently two main models regarding the origin of the hemispherical inner core structure. In the first, thermochemical coupling between the inner core and the mantle is proposed to result in an asymmetry of growth rates [*Aubert et al.*, 2008]. This corresponds to greater heat extraction in the east hemisphere,

resulting in faster crystallization which generates the seismic differences. The second theory suggests that the inner core undergoes lateral translation, driven by melting of the east hemisphere and crystallization of the west [*Alboussiére et al.*, 2010; *Monnereau et al.*, 2010]. Neither of these processes is able to reproduce all of the seismic observations. In particular, the observation of sharp hemisphere boundaries [*Waszek and Deuss*, 2011] and the depth variation of anisotropy have proven challenging to both models [*Geballe et al.*, 2013]. If the hemispherical variation is due to solidification, then we would expect the hemispherical differences to continue up to the ICB. Thus, constraining the seismic properties right at the ICB is essential to determine the mechanism which generates the hemispherical differences.

Here we will study seismic structure at the ICB directly by using the seismic compressional phase *PKiKP*, which travels through the mantle and outer core and then reflects from the ICB. The travel time of *PKiKP* is linked to seismic velocity in the outer core and the radius of the inner core, and its amplitude is affected by the impedance contrast at the ICB. Unfortunately, it is not straightforward to detect this phase. Heterogeneity and strong attenuation in the mantle both have a large influence on the *PKiKP* amplitude, resulting in a small signal magnitude. This is exacerbated by the already small theoretical amplitude of *PKiKP* at subcritical distances [*Shearer and Masters*, 1990; *Cao and Romanowicz*, 2004a]. Even when *PKiKP* is observed, the effects of mantle structure are difficult to remove [*Koper et al.*, 2003; *Koper and Pyle*, 2004; *Tkalĉic et al.*, 2009].

The first observations of *PKiKP* at steep incidence confirmed that the inner core boundary is sharp, of thickness less than 1–2 km [*Bolt and Qamar*, 1970; *Engdahl et al.*, 1970]. Subsequent studies used *PKiKP* to calculate the density jump across the inner core boundary, and this has remained a topic of debate to the present day. Observed values range widely, from 1.6 to 1.8 g cm^{-3} [*Bolt and Qamar*, 1970; *Souriau and Souriau*, 1989], to 0.9 g cm^{-3} [*Bolt*, 1972; *Cao and Romanowicz*, 2004b] and as low as 0.45 g cm^{-3} [*Koper and Pyle*, 2004]. *Tkalĉic et al.* [2009] proposed density contrasts varying from 0.2 to 1.1 g cm^{-3}, with large regional differences. This may explain some of the discrepancy in previous observations. Additionally, an observation bias may be introduced, whereby *PKiKP* is only observed when it has a large amplitude [*Shearer and Masters*, 1990]. This is corroborated by normal mode results, which predict a smaller density contrast than several body wave studies; *Shearer and Masters* [1990] found that normal modes indicate a density jump of 0.55 g cm^{-3}.

Previous inner core studies have suggested the presence of a hemispherical difference in velocity contrast at the ICB in *PKIKP-PKiKP* travel time residual data [*Wen and Niu*, 2002; *Yu and Wen*, 2006]. Hemispherical structure at the boundary has not been observed directly, however. Instead, only smaller scale regional variations have been detected in *PKiKP* travel times and amplitudes [*Koper and Dombrovskaya*, 2005]. Some studies propose that these arise from structure on the boundary itself. One possibility is ICB topography [*Wen*, 2006], although its magnitude displays large variations between regions. Seismic doublets have been used to infer ICB topography of less than 0.5 km [*Cao et al.*, 2007], whereas more recent work proposed topography of up to 14 km [*Dai et al.*, 2012] on lateral length scales of less than 10 km. Conversely, another *PKiKP* study suggested that the ICB comprises a mosaic of interspersed fluid and solid regions, in order to explain large differences in *PKiKP* amplitude [*Krasnoshchekov et al.*, 2005]. *Leyton and Koper* [2007] determined that scattering from heterogeneities in the upper 350 km of the inner core strongly influence *PKiKP* coda. On the other hand, the authors found that core-mantle boundary (CMB) topography produces large difference in the *PKiKP* amplitudes. *Koper et al.* [2003] also preferred topography of up to 3.5 km on the CMB rather than the ICB to explain seismic observations of *PKiKP*.

Alternatively, regional differences in *PKIKP-PKiKP* travel times and *PKiKP*/*PcP* amplitude ratio data may originate from the *F* layer instead. This is a boundary layer that extends up to 300 km above the ICB, in which inner core solidification is proposed to occur [*Gubbins et al.*, 2008]. The layer is suggested to be compositionally distinct to the bulk of the outer core, with higher density and viscosity due to an increased solid fraction. As a consequence, it may be able to sustain laterally varying structure [*Cormier*, 2009]. Such regional variations may be linked to compositional differences, which result from crystallization or melting of the inner core [*Gubbins et al.*, 2011]. Identifying the cause of any regional features is thus particularly important as they are linked to the solidification properties of the inner core.

Here we investigate the structure on and above the ICB, using a large data set of *PKiKP* and *PcP* phases. Previous studies suffered from a lack of data, and we benefit from significant improvement in global seismic coverage over the last few years. We examine the *PKiKP*/*PcP* amplitude ratios, which may provide information regarding the impedance contrast of the ICB. We also measure the *PKiKP-PcP* differential travel time residuals to study

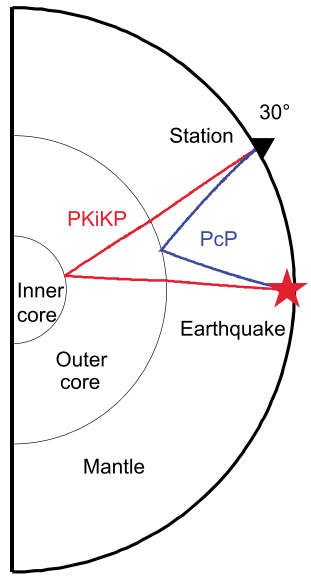

Figure 1. Raypaths of *PKiKP* (red) and *PcP* (blue) for an event at 100 km depth.

velocity in the *F* layer and topography on the ICB. Our goal is to understand any relationship between seismic velocity and impedance at the ICB and the properties of the material beneath it.

2. Data and Methods

2.1. Data

We study the ICB and the *F* layer using *PKiKP*, a compressional phase which travels through the mantle and outer core, and reflects from the ICB. As a reference phase, we use *PcP*, a compressional phase which reflects from the core-mantle boundary (CMB) (Figure 1). These phases may be observed simultaneously at epicentral distances from 0 to 70°. We require events with source depths greater than 50 km, to avoid surface reflections, and magnitude $M_w \geq 5.5$, to generate observable phases. We collected data from all events which fulfill this criteria from January 2000 to December 2013, in addition to several nuclear explosions from the 1990s. This provides a total of 1053 events, with an initial data set of over 170,000 seismograms.

We band-pass filtered the data between 0.7 and 3 Hz. For quality purposes, we perform a visual inspection of each seismogram before picking and require that *PKiKP* and *PcP* are clearly visible with no other phases predicted to arrive or present within 10 s of either phase. The phases are then picked using cross correlation of *PKiKP* with *PcP* and checked manually. Using Seismic Analysis Code [*Goldstein et al.*, 2003], we measured the travel time differential and peak-to-peak amplitude of the phases. With the amplitudes, we determine the *PKiKP*/*PcP* amplitude for each seismogram. After quality checking, our final data set totals 167 seismograms with clear *PKiKP* and *PcP* arrivals, which is the largest global hand-picked data set of *PKiKP-PcP* data. The small percentage of seismograms which we retain from the original data set is less than 0.1%, which highlights their quality. We also collected 157 seismograms which show a clear *PcP* arrival and minimal noise, yet have no *PKiKP* signal. The noise level at the predicted arrival time of *PKiKP* provides an upper bound on its amplitude.

Figure 2 shows examples of our observed seismograms. We show the full seismogram and trimmed seismograms within ±10 s of *PcP* and *PKiKP*. The epicentral distance and observed and theoretical *PKiKP*/*PcP* amplitude ratio are included in each panel. Additional major mantle phases within the full seismogram have been identified. The AK135 predicted arrival times are marked by black dashed lines. Figures 2a–2h show seismograms which have clear *PcP* and *PKiKP* signals, for a range of epicentral distances and amplitude ratios. In many cases, the amplitude ratios are either close to predicted values (Figures 2a and 2b) or slightly larger (Figures 2c and 2d) or smaller (Figure 2e) than predicted. However, in some instances we find two seismograms with very different amplitude ratios (0.06 compared to 0.36), yet they are from the same event with similar travel paths and reflection points at the CMB and ICB. This highlights the large differences in amplitudes over small lateral length scales. Figures 2g and 2h are examples of data with significantly larger amplitude ratios than predicted. Finally, Figures 2i and 2j show examples of a clear *PcP* arrival with minimal noise, but no *PKiKP* signal. Here the observed amplitudes ratios are very close to the predictions.

2.2. *PKiKP*/*PcP* Amplitude Modeling

We calculate theoretical *PKiKP*/*PcP* amplitude ratios as a function of epicentral distance, using the method outlined in *Tkalčic et al.* [2009]. We incorporate geometrical spreading of both phases, attenuation in the outer core, and reflection and transmission coefficients at the CMB and ICB. The reflection and transmission coefficients take into account the contrasts of compressional wave velocity, shear wave velocity, and density across the boundaries.

The theoretical *PKiKP*/*PcP* amplitude ratio is given by the following equation [*Tkalčic et al.*, 2009]:

$$A = \frac{T_{PKiKP} R_{PKiKP} T_{PKiKP}}{R_{PcP}} \Big/ \frac{\eta_Q}{\eta_S} \tag{1}$$

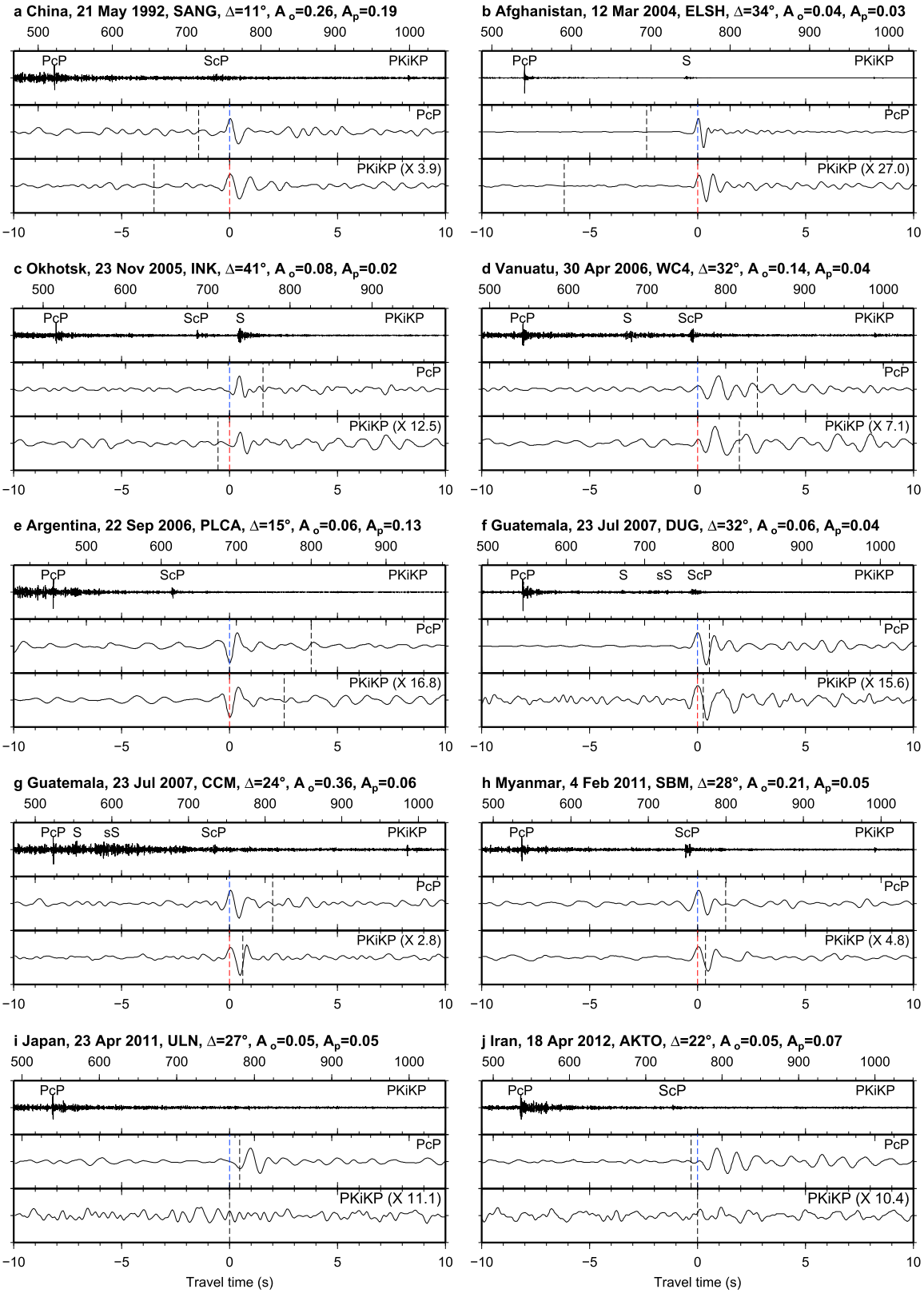

Figure 2. (a–j) Narrow band-passed displacement seismograms showing examples of *PKiKP* and *PcP* observations, with the full seismogram for reference. The *PcP* and *PKiKP* panels are aligned to our picked arrival times, which are marked by blue and red dashed lines, respectively. Observed and theoretical amplitude ratios (calculated using equation (1)) are included. Very large amplitude signals are shown in Figures 2g and 2h. Examples of a clear *PcP* arrival with no corresponding *PKiKP* signal are shown in Figures 2i and 2j.

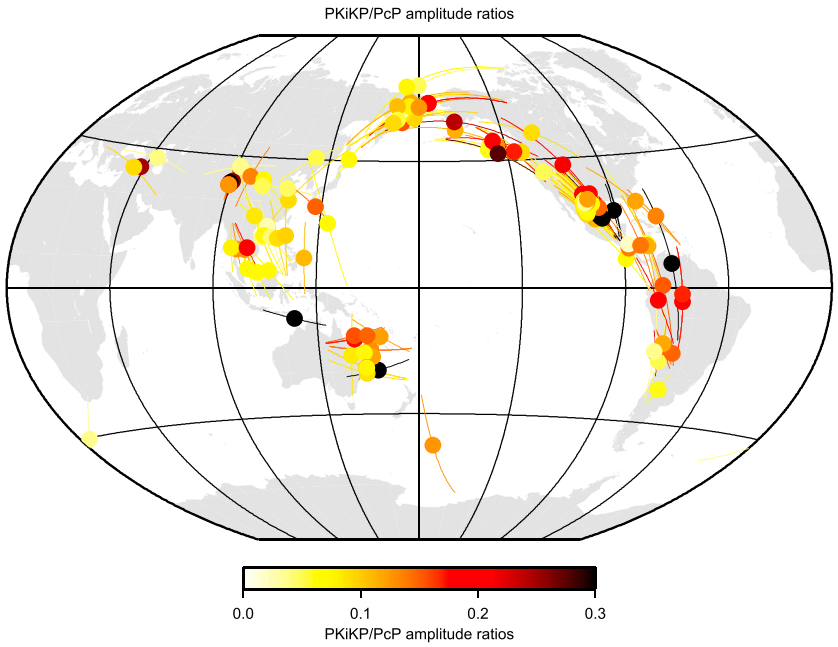

Figure 3. Global map of *PKiKP*/*PcP* amplitude ratios. Lines represent *PKiKP* raypaths through the outer core, circles correspond to *PKiKP* bounce points on the ICB. Some consistent regional variation may be observed; for example, beneath Southeast Asia. However, the majority of the data shows large amounts of scatter, and no hemispherical difference can be detected. This is consistent with *PKIKP*/*PKiKP* amplitude ratio data [*Waszek and Deuss*, 2013].

where T and R are transmission and reflection coefficients of *PKiKP* and *PcP* at the CMB and ICB. Attenuation and geometrical spreading are denoted by η_Q and η_S, respectively. Outer core attenuation, η_Q, is given by

$$\eta_Q = e^{-\pi\delta t/QT} \tag{2}$$

where δt is the travel time of *PKiKP* in the outer core, Q is the quality factor in the outer core (taken as 10,000), and T is the period of *PKiKP*. The ratio of geometrical spreading factors for *PKiKP* and *PcP* is η_S, calculated as follows:

$$\eta_S = \sqrt{\frac{\cos^2(i_{PKiKP})}{\cos^2(i_{PcP})}\frac{p_{PcP}}{p_{PKiKP}}\left|\left(\frac{\mathrm{d}p}{\mathrm{d}\Delta}\right)_{PcP}\Big/\left(\frac{\mathrm{d}p}{\mathrm{d}\Delta}\right)_{PKiKP}\right|} \tag{3}$$

where i is the incident angle at the respective boundary, p is slowness, and Δ is epicentral distance.

Our previous work has shown that a small difference in velocity contrast at the ICB will have a large influence on *PKIKP*/*PKiKP* amplitude ratios [*Waszek and Deuss*, 2013]. Here we will investigate the effects of a hemispherical difference in seismic velocity at the ICB on *PKiKP*/*PcP* amplitudes, by extending the velocity model from *Waszek and Deuss* [2011] up to the ICB, and using it to calculate the *PKiKP* reflection coefficient. We will also explore the influence of altering density contrast at the ICB and the CMB.

The earthquake radiation pattern may have a significant effect on the amplitude of the phases, if the phases emanate from close to a nodal plane. *PKiKP* and *PcP* have different takeoff angles, and the difference between their takeoff angles increases with epicentral distance; the maximum difference in our data is approximately 8°. We check for the influence of the radiation pattern by generating synthetic seismograms for every observed seismogram, using WKBJ ray tracing [*Chapman*, 1976] for the appropriate Centroid Moment Tensor (CMT) solution [*Ekström et al.*, 2005]. Any seismograms which have anomalously large theoretical *PKiKP*/*PcP* amplitude ratios as a result of the radiation pattern are removed.

2.3. *PKiKP-PcP* Differential Travel Times

The differential travel time residuals between *PKiKP* and *PcP* are calculated with respect to predictions for the 1-D Earth model AK135 [*Kennett et al.*, 1995] and are defined as

$$\Delta t = (PKiKP_{\mathrm{obs}} - PKiKP_{\mathrm{pred}}) - (PcP_{\mathrm{obs}} - PcP_{\mathrm{pred}}) \tag{4}$$

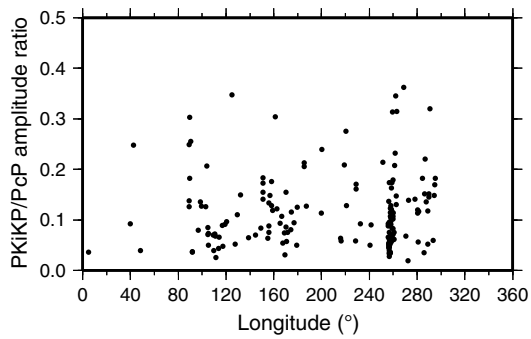

Figure 4. Observed *PKiKP*/*PcP* amplitude ratios as a function of *PKiKP* bounce point longitude.

A negative travel time residual therefore corresponds to an early arrival of *PKiKP* or a late arrival of *PcP*. The separation between takeoff angles introduces errors to the travel time residuals, due to the path difference through the mantle. We correct the residuals for 3-D mantle velocity structure using the MITP08 model [*Li et al.*, 2008] and for ellipticity of the Earth.

3. Observations

3.1. *PKiKP*/*PcP* Amplitude Ratios

We first examine a map of the *PKiKP*/*PcP* amplitude ratios (Figure 3). There is a large amount of scatter in the data, and we do not observe hemispherical structure in the map. We note, however, that there is some regional consistency. For example, there are more data with large-amplitude ratios (red points) beneath Central and South America and more data with smaller amplitude ratios (yellow points) beneath Asia. The data beneath Asia also show less scatter. Next, we examine the amplitude ratios as a function of *PKiKP* bounce point longitude, to investigate whether we can observe any hemispherical difference in the data (Figure 4). We find that the data show large amounts of scatter throughout, and there is no evidence for a hemispherical difference in this data. However, this figure does not account for the strong dependence of amplitude ratio on epicentral distance.

We now compare our observed amplitude ratios as a function of epicentral distance to theoretical predictions in Figure 5. The theoretical amplitude ratios are calculated by extending our hemispherical velocity structures to the top of the inner core, with $v_p = 11.1297$ km s^{-1} in the east and $v_p = 10.9896$ km s^{-1} in the west [*Waszek and Deuss*, 2011]. This corresponds to jumps across the ICB of 0.8407 km s^{-1} and 0.7006 km s^{-1}, respectively.

The theoretical amplitudes decrease as a function of epicentral distance. When *PKiKP* is detected, we find that the observed *PKiKP*/*PcP* amplitudes are much larger than the theoretical predictions, and they do not appear to depend on epicentral distance (Figure 5a). Anomalously large-amplitude ratios have previously been detected at regional levels by *Koper and Pyle* [2004] and *Dai et al.* [2012]. *Shearer and Masters* [1990] suggested that precritical *PKiKP* is only observable in exceptional circumstances, for example, if there is significant focusing to increase the signal amplitude. The scatter in the observed data is much larger than the predicted difference between east and west, showing that we would not be able to distinguish a hemispherical variation in velocity jump at the ICB even if it existed.

The binned data confirm that neither hemisphere has consistently larger amplitude ratios (Figure 5b). Instead, the averages show much variability, and the standard deviations overlap significantly. Our hemispherical models here are in Δv_p and do not include differences in $\Delta\rho$. Since compressional velocity and density are inversely related, if the hemispherical differences are compositional in origin, we would expect a decrease in ρ to accompany an increase in v_p. This would mean any hemispherical variation in reflection coefficient at the ICB would be even smaller than the values in Figure 5.

In order to investigate the possibility that we only detect anomalously large *PKiKP* signals, we also plot amplitude ratios from data with high-quality *PcP* arrivals but no visible *PKiKP* signals (Figure 5c). Here we measure the noise level at the predicted *PKiKP* arrival time to obtain an upper bound on the *PKiKP*/*PcP* amplitude ratio. These data are much closer to the theoretical values, which is consistent with observations by *Shearer and Masters* [1990]. Although some individual data are still larger than the theoretical values, the majority of binned averages are within a standard deviation of the predictions (Figure 5d). This indicates that the *PKiKP* phases we observe have atypically large amplitudes, as suggested by *Shearer and Masters* [1990].

Some of the large *PKiKP*/*PcP* amplitude ratios may result from random noise increasing the amplitude of *PKiKP*. We investigate this possibility by measuring the maximum peak-to-peak amplitude in the 10 s preceding the *PKiKP* arrival, which provides a measure of quality for each data point. The *PKiKP* noise/*PKiKP* amplitude ratios for the observed data are shown in Figure S1 in the supporting information. Darker colors correspond to lower noise/*PKiKP* ratios, meaning that the noise near *PKiKP* is lower amplitude, and hence, the *PKiKP* amplitude is more reliable. Conversely, lighter colors mean that the seismogram has higher noise amplitudes near to

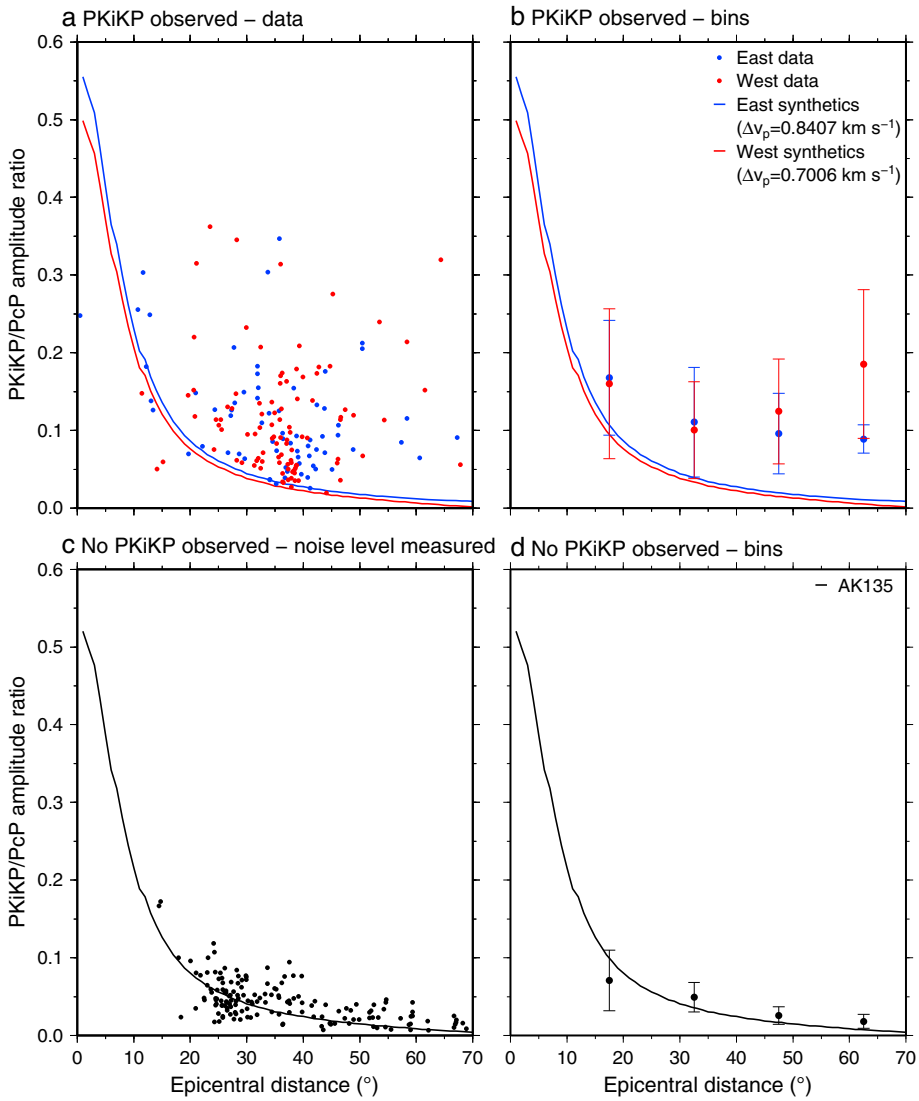

Figure 5. Observed *PKiKP*/*PcP* amplitude ratios as a function of epicentral distance, with theoretical values predicted from hemispherical velocity contrasts at the ICB. The data are separated into hemispheres by *PKiKP* reflection points on the ICB, using the hemisphere boundaries determined in *Waszek et al.* [2011]. (a and b) *PKiKP* observed. (c and d) No *PKiKP* observed—noise level at predicted *PKiKP* time measured. Figures 5a and 5c show individual data points, and Figures 5b and 5d show average amplitude ratios for epicentral distance bins of 15°. The error bars represent standard deviation.

PKiKP, and thus, *PKiKP* may be affected by noise. We find that there is no correlation between large *PKiKP*/*PcP* amplitude ratios and high *PKiKP* noise levels. Indeed, the largest observed *PKiKP*/*PcP* amplitude ratio has minimal noise near *PKiKP*, and the majority of data have low noise levels. Random noise will also decrease the *PKiKP* amplitudes for some data and will affect the *PcP* amplitudes. Some data which are smaller than theoretical predictions have large *PKiKP* noise levels. Thus, random noise is unlikely to be the major cause of the anomalously large-amplitude ratios.

Next, we determine the influence of focal mechanisms on the amplitude ratios with WKBJ [*Chapman*, 1976], calculating theoretical *PKiKP*/*PcP* amplitude ratios for every seismogram, using the appropriate CMT solution [*Ekström et al.*, 2005]. Comparing the WKBJ theoretical amplitude ratios to the calculated theoretical amplitude ratios (Figure 6), we find that the WKBJ data display a small amount of scatter but cannot explain the anomalously large data. WKBJ does not include attenuation, and so the theoretical amplitude ratios for AK135 without attenuation matches the WKBJ amplitudes much more closely than the theoretical values which include attenuation. Some of the WKBJ amplitudes are still significantly larger than the theoretical calculations,

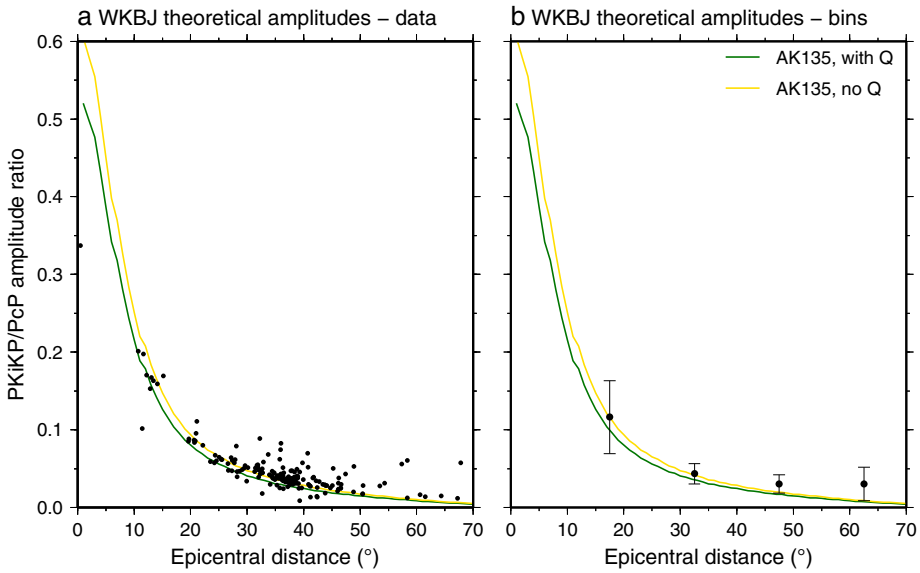

Figure 6. Theoretical *PKiKP*/*PcP* amplitude ratios as a function of epicentral distance, calculated for each data point using WKBJ [*Chapman*, 1976] with the appropriate CMT solutions [*Ekström et al.*, 2005]. Theoretical values predicted from AK135 are included as before (green line). We also show theoretical values predicted for AK135 without outer core attenuation, since WKBJ does not model attenuation (orange). (a) Individual data points and (b) average amplitude ratios for epicentral distance bins of 15°. The error bars represent standard deviation.

however, which skews the average bins. This likely results from the CMT focal mechanism. Previously, we removed any data for which the WKBJ theoretical *PKiKP*/*PcP* amplitudes were anomalously large as a result of the focal mechanism. These amplitude ratios were in excess of 0.4, and thus, errors in the CMT solution may be able to account for the extrema in our data. However, the majority of our *PKiKP*/*PcP* amplitude ratio data are consistently larger than can be predicted by any ICB or CMB velocity model, or by WKBJ. Hence, erroneous focal mechanisms cannot be the sole explanation for our observations.

We examine the influence of varying density contrast at the ICB in Figure 7, from 0.0 to 2.0 kg m^{-3}. The density contrast in AK135 is 0.6 kg m^{-3} (green line). None of the density models predict amplitude ratios large enough to explain the observed data averages, and many observed amplitude ratios are significantly larger than the theoretical values (Figure 7a). For data in which *PKiKP* is not detected, the majority of observed amplitude ratios are close to the theoretical values (Figure 7b). All of the binned averages are lower than theoretical values for a density jump of 1.6 kg m^{-3}. This indicates an observational bias: we only detect *PKiKP* when it is above the noise level and therefore has a larger amplitude than average. The amplitude ratios from the *PKiKP* noise level data provides an approximate upper bound on the ICB density contrast. We use a least squares method to calculate that an ICB density jump of 1.2 kg m^{-3} is the best fit to our data in Figure 7b. This is twice the density jump in AK135, suggesting that *PKiKP* would be expected to have a smaller amplitude than the noise.

Altering the compressional velocity contrast at the ICB has similar results to changing the density contrast; an increase in either produces an increase in *PKiKP* amplitude. We vary the compressional velocity from 0.4 to 1.6 km s^{-1} in Figure S2. As with density, none of the models can generate amplitude ratios as large as the observed data averages, and many are much larger than the theoretical values (Figure S2a). Conversely, the data in which *PKiKP* is not detected have amplitude ratios much closer to the predictions (Figure S2b). Here the binned averages suggest an upper bound on the velocity contrast of 1.2 km s^{-1}. Employing the least squares method, we determine that a velocity jump of 0.9 km s^{-1} best fits our data in Figure S2b. This is again larger than AK135.

The large *PKiKP* amplitudes are difficult to explain with ICB structure, so we next investigate the effects of varying density contrast at the CMB (Figure 8), from 3.6 to 6.0 kg m^{-3}, also encompassing the AK135 density contrast of 4.4 kg m^{-3} (green line). Again, we find that all of these models predict *PKiKP*/*PcP* amplitude ratios which are too small to explain most of our observed data (Figure 8a). Most of the binned average amplitude ratios are significantly larger than the theoretical values. As in Figure 7, we observe a much better match to

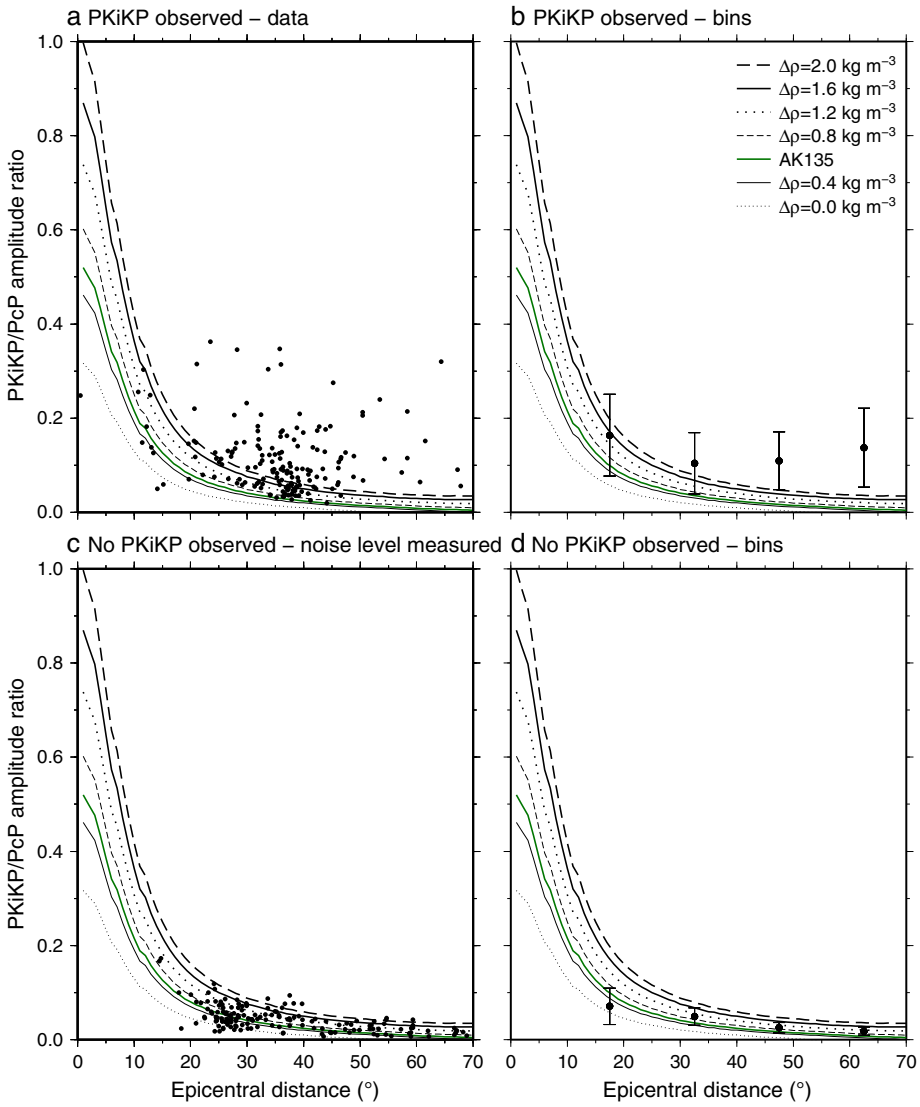

Figure 7. Observed *PKiKP*/*PcP* amplitude ratios as a function of epicentral distance, with theoretical values from varying density contrasts at the ICB. The green line is the density contrast for AK135. (a and b) *PKiKP* observed. (c and d) No *PKiKP* observed—noise level at predicted *PKiKP* time measured. Figures 7a and 7c show individual data points, and Figures 7b and 7d show average amplitude ratios for epicentral distance bins of 15°. The error bars represent standard deviation.

the predictions when *PKiKP* is not detected (Figure 8b). If the large *PKiKP* amplitudes cannot be explained by either ICB or CMB density contrasts, they must be generated by an alternative mechanism. Structure at the ICB can produce anomalously large *PKiKP* amplitudes, for example, as a result of interspersed solid and fluid regions [*Krasnoshchekov et al.*, 2005], or focusing from small length scale topography [*Dai et al.*, 2012]. Conversely, *Tkalčic et al.* [2010] found that such large variations in *PKiKP*/*PcP* amplitudes can be explained by focusing in the shallow mantle. Heterogeneity beneath receivers which has scale lengths oriented parallel to the incoming raypaths can produce significant differences in amplitude [*Zheng and Wu*, 2008; *Hong and Menke*, 2008; *Tkalčic et al.*, 2010]; this will particularly affect receivers above subduction zones.

We therefore consider a map of the *PKiKP*/*PcP* amplitude ratios as a function of receiver location (Figure S3). This is in order to determine whether areas with significant scatter or very large *PKiKP*/*PcP* amplitude ratios are associated with receivers above subduction zones. We plot the data at the CMB exit points of the *PKiKP* ray, so that the incoming rays for each station do not overlap. Examining the region around the Pacific, we find that many of the receivers with the largest amplitude ratios are located above subduction zones. This is in agreement with the observations of *Tkalčic et al.* [2010]. Stations in the Kurile, Aleutian, and South American regions

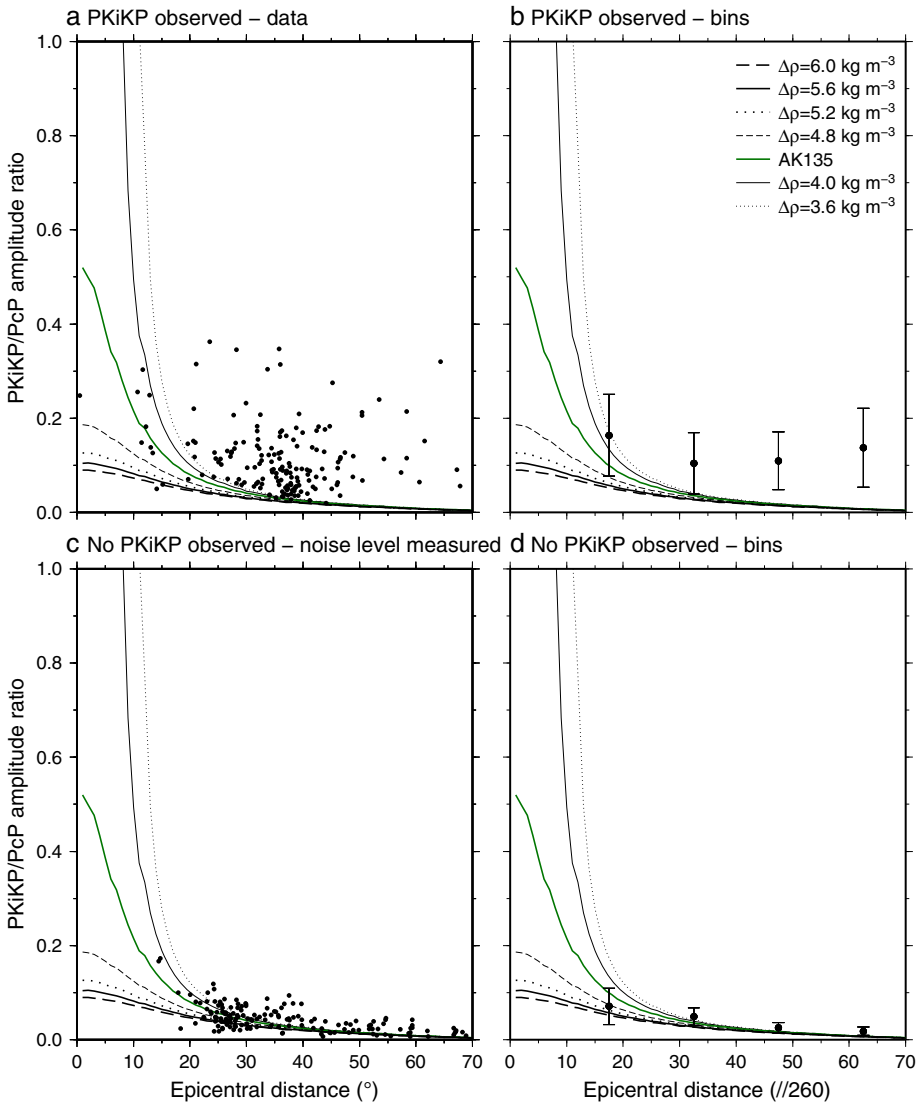

Figure 8. Observed *PKiKP*/*PcP* amplitude ratios as a function of epicentral distance, with theoretical values from varying density contrasts at the CMB. The green line is the density contrast for AK135. (a and b) *PKiKP* observed. (c and d) No *PKiKP* observed—noise level at predicted *PKiKP* time measured. Figures 8a and 8c show individual data points, and Figures 8b and 8d show average amplitude ratios for epicentral distance bins of 15°. The error bars represent standard deviation.

display a wide range of amplitude ratio values; however, the South West Pacific has primarily small-amplitude ratios, and Central America primarily large ratios. A lack of receivers above other subduction zones prevents further investigation. Data with large-amplitude ratios are also found outside of the subduction zones; however, the few number of receivers and sparse coverage here means that it is difficult to make a meaningful comparison.

3.2. *PKiKP-PcP* Differential Travel Time Residuals

We now consider the differential travel time residuals of *PKiKP* and *PcP*. A negative travel time residual corresponds to an earlier arrival of *PKiKP* or a late arrival of *PcP*. In the map of the *PKiKP-PcP* residuals (Figure 9), we observe large-scale regional differences. We find paths with more negative residuals beneath Russia and Alaska and paths with less negative values beneath Central and South America. However, we do not observe an obvious hemispherical difference.

In order to confirm that these variations arise from *PKiKP* and not *PcP*, we plot the differential residuals as a function of *PcP* residuals and of *PKiKP* residuals (Figure 10). There is no relationship between the differential

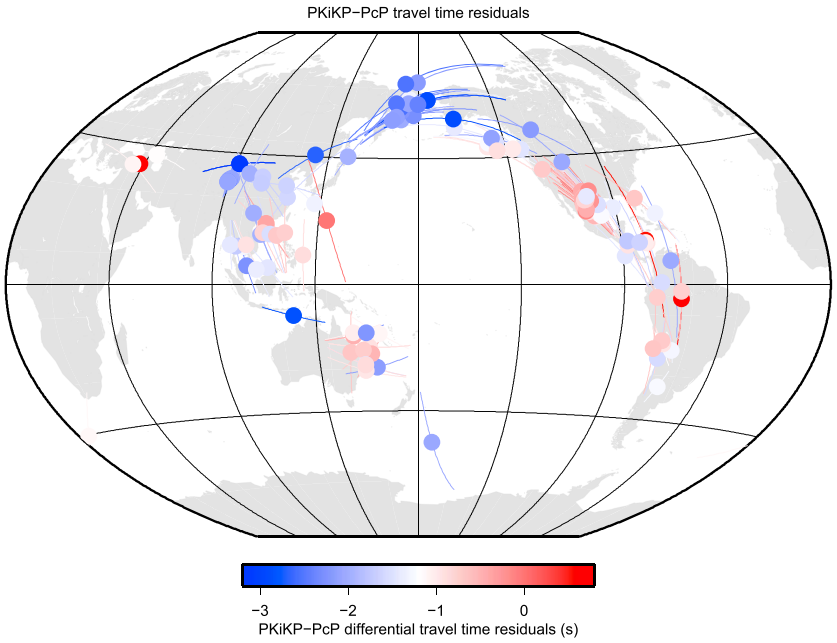

Figure 9. Observed *PKiKP*/*PcP* differential travel time residuals with respect to AK135. Lines represent *PKiKP* raypaths through the outer core, circles correspond to *PKiKP* bounce points on the ICB.

residuals and the *PcP* residuals (Figure 10a). There is a positive correlation with the *PKiKP* residuals (Figure 10b), implying that the variation in *PKiKP-PcP* residuals results from *PKiKP*. Any correlation between the residuals and mantle structure would affect both *PcP* and *PKiKP* residuals; thus, the variations in our residuals can be attributed to structure in the outer core and the ICB.

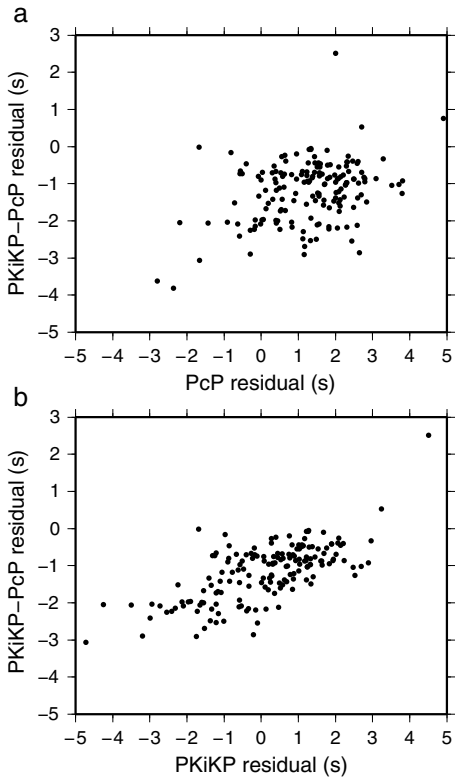

Figure 10. Observed *PKiKP-PcP* differential travel time residuals as a function of (a) *PcP* residuals and (b) *PKiKP* residuals.

Next, we examine the residuals as a function of epicentral distance (Figure 11a), which is a proxy for travel time in the outer core. There is no correlation between residual and epicentral distance, indicating that the variation is not a consistent function of travel time in the outer core or the *F* layer. We find that the spread in the residuals increases for larger epicentral distances, corresponding to increasing difference between the mantle paths of *PKiKP* and *PcP*. This means that some scatter in our data likely results from mantle structure. The overall average residual is −1.19 s, indicating that in AK135 either the thickness of the outer core is too large by approximately 6 km (i.e., the inner core radius is too small, or outer core radius is too large) or the average velocity in the outer core is too low by 0.25%.

We investigate the possibility of hemispherical variation in our travel time data in more detail in Figure 11b, examining the *PKiKP-PcP* residuals as a function of *PKiKP* bounce point longitude. Taking the hemisphere boundaries as before, we calculate that the average residual is −1.46 s for the east hemisphere and −1.06 for the west hemisphere. We use a *t* test to determine that this difference is statistically significant at the 1% level. However, we note that there is much scatter in the data, and the averages are dominated by clusters

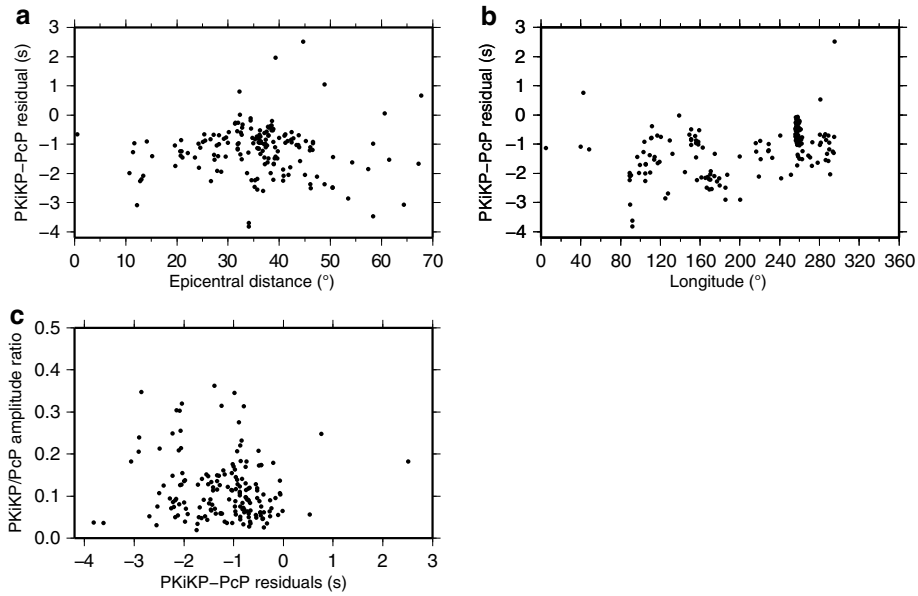

Figure 11. (a) Observed *PKiKP-PcP* differential travel time residuals as a function of epicentral distance. (b) Observed *PKiKP-PcP* differential travel time residuals as a function of *PKiKP* bounce point longitude. (c) Observed *PKiKP*/*PcP* amplitude ratios as a function of observed *PKiKP-PcP* differential travel time residuals.

of data (for example, at ~230°). Figure 9 shows that this apparent hemispherical difference is more likely to result from the strongly varying regional structure, rather than distinct hemispheres.

In order to search for localized variations in our data, we examine the regions with highest data density in more detail (Figure 9). We consider three regions: Russia and Alaska, Southeast Asia and Australia, and North and South America. The average residual beneath Russia and Alaska is −2.04 s but only −1.49 s beneath Southeast Asia and Australia, and an even smaller value of -0.86s is found beneath the Americas. Our observations are in excellent agreement with a previous *PKiKP-PcP* study by *Koper et al.* [2003], who found similar differences in travel time residuals between these locations.

Within each region, we observe lateral variations of up to 4 s over distances as small as ~100–200 km, in good agreement with previous studies. Examining the regions in Figure 9 in detail, we also find that the amount of scatter varies between regions. The area beneath Russia and Alaska contains primarily strongly negative travel time residuals, with little scatter in the data. Asia and Australia show greater variation, but the largest scatter on short length scales is found under the Americas. The region beneath Central America, in particular, displays large differences in travel time residual across small lateral distances. Some of the scatter may result from mantle heterogeneity; however, Figure 10 shows that the main trend in residuals results from *PKiKP*, and therefore the outer core and ICB. The different magnitudes of scatter may therefore correspond to topography on the ICB [*Wen*, 2006; *Cao et al.*, 2007; *Dai et al.*, 2012], velocity variations in the *F* layer [*Cormier*, 1999], or a combination.

We find that there is no correlation between the *PKiKP*/*PcP* amplitude ratios and travel time residuals (Figure 11c). The amplitude ratio depends primarily on the reflection and transmission coefficients at the CMB and ICB, whereas the travel time residuals result from velocity and thickness of the outer core. Our observation therefore suggests that there is no global relationship between these two features.

4. Discussion

4.1. Amplitude Ratios

Many of our observed *PKiKP*/*PcP* amplitude ratios are much larger than predicted by AK135. They cannot be explained by varying density contrasts across either the ICB or CMB, errors in focal mechanism, or noise near *PKiKP*. Conversely, amplitude ratios measured using the noise level when *PKiKP* is not observed are much smaller and closer to the theoretical values. Our results suggest that we only observe *PKiKP* when it is anomalously large and therefore visible above the noise level, due to focusing along its raypath. We do not observe

a hemispherical difference in the amplitude ratios and determine that it would not be possible to detect even if it existed, due to strong scatter in the data.

Large variation in *PKiKP* amplitudes has been suggested to arise from a mosaic structure of fluid and solid on the ICB [*Krasnoshchekov et al.*, 2005] or from focusing by ICB topography [*Dai et al.*, 2012]. Heterogeneities in the upper inner core may also affect the *PKiKP* amplitudes [*Poupinet and Kennett*, 2004; *Koper and Dombrovskaya*, 2005; *Leyton and Koper*, 2007]. Amplitudes of seismic phases depend on their entire travel paths through the Earth. The separation of *PKiKP* and *PcP* at the CMB is over 23° for the largest epicentral distance we use (68°), which corresponds to a lateral distance of 1160 km. Strong variations occur in the mantle on length scales of less than 50 km [*Hedlin and Shearer*, 2000]. Such structures include ancient subducted slabs, partial melt, and ultralow velocity zones (ULVZs) [*Ritsema et al.*, 2004; *Hutko et al.*, 2006; *McNamara et al.*, 2010].

Despite the *PKiKP* and *PcP* raypaths being most similar in the crust, small-scale heterogeneities here can cause large variation in *PKiKP*/*PcP* amplitude ratios [*Zheng and Wu*, 2008; *Hong and Menke*, 2008]. This is proposed to arise due to heterogeneity beneath receivers with scale lengths oriented in the direction of travel of the rays, which results in stronger attenuation of *PcP* than *PKiKP* due to backscattering [*Tkalčic et al.*, 2010]. A problem with our data coverage is that many of our stations are located above subduction zones, meaning that we cannot make significant comparisons with a range of nonsubduction areas. We find large-amplitude ratios for stations both above and outside of subduction zones. Some subduction areas have receivers with widely varying amplitude ratios, whereas others do not. Thus, although heterogeneity in the crust likely has some influence on our amplitude ratios, it cannot explain all of our observations.

We suggest that the wide range of scatter in the amplitude ratio data is a result of the path differences through the Earth and heterogeneities beneath the receivers. Additionally, large *PKiKP* amplitudes may be generated by focusing due to small-scale topography on the ICB. This ICB topography will also influence the small-scale travel time residual data.

4.2. Travel Time Residuals

In the travel time residuals, we detect differences of up to 1.24 s between the averages for the large regions (Figure 9). We also observe variations within each of these regions, with a spread in residual of up to 1.5 s on length scales of ~100–200 km. The differences may result from ultralow velocity zones (ULVZs), velocity variations in the *F* layer, ICB topography, or a combination and will discuss these in detail below.

4.2.1. ULVZs

Very anomalous *PKiKP-PcP* travel time residuals have been proposed to result from ULVZs [*Koper et al.*, 2003]. These would result in large *PcP* residuals, in combination with very negative *PKiKP-PcP* residuals, which we do not observe. Comparing our data to a map of ULVZs [*McNamara et al.*, 2010], we find no correlation between locations of ULVZs and extrema in the *PKiKP-PcP* data. For example, no ULVZs have been found beneath Central America, where we find much scatter in our data. On the other hand, subducted slab remnants have been detected in this region [*Cao et al.*, 2007; *Miller and Niu*, 2008], which may produce some of the short length scale variations we observe [*Vanacore et al.*, 2010]. Since the *PKiKP-PcP* residual times show a clear correlation with *PKiKP* arrival time (Figure 10), we believe that the main influence must be outer core and/or ICB structure instead.

4.2.2. Velocity Variations in the *F* Layer

For an *F* layer thickness of 300 km, 0.1 s of travel time variation for *PKiKP* corresponds to ~0.25% perturbation in compressional velocity. If we attribute the variations in travel time residuals entirely to the *F* layer, we require velocity differences of up to 3% between the large regions and up to 4% to explain small-scale scatter. Given the low viscosity of the outer core, it is unlikely that strong heterogeneity of 4% would be sustained over the small length scales of less than 200 km. Larger regional variations in velocity may exist in the *F* layer, however, with the requirement that the viscosity is higher than the bulk of the outer core. Compositional differences generated from freezing or melting of the inner core will alter the seismic velocity above the ICB. For example, a rapid growth of the inner core and its corresponding release of light elements would decrease the density in the *F* layer, increasing its compressional velocity. Conversely, localized melting produces denser fluid, thereby decreasing the compressional velocity [*Badro et al.*, 2007; *Antonangeli et al.*, 2010].

Only temporal consistency in the solidification and melting patterns of the inner core is needed to maintain regional differences. This would be compatible with the geodynamic model of long-term thermochemical coupling between the inner core and mantle [*Aubert et al.*, 2008]. Regional variations in ICB heat flux would

generate localized seismic anomalies in the inner core [*Gubbins et al.*, 2011], which have been observed in the upper inner core [*Waszek and Deuss*, 2011]. Comparing these ideas with our observations indicates greater heat extraction and faster solidification beneath Russia and Alaska, leading to faster compressional velocity in the *F* layer. Slower heat loss, or even inner core melting, would occur beneath Central America, producing lower velocity. Hence, we suggest that the large-scale regional differences result from the *F* layer. Solidification and melting of the ICB will also affect its topography and reinforce the influence on the travel time residuals.

Velocity variations in the *F* layer will also influence the *PKiKP*/*PcP* amplitude ratios, by altering the velocity jump at the ICB. A decrease of 3% in the *F* layer corresponds to an ICB velocity contrast of 1.06 km s^{-1}, and a decrease of 4% gives a contrast of 1.16 km s^{-1}. This will therefore increase the amplitude ratios, as per Figure S2. However, these velocity jumps cannot match the very large amplitudes of the observed data, and thus, the velocity variations in the *F* layer would have a significant effect for only the travel time residuals.

4.2.3. Topography on the Inner Core Boundary

Travel time residuals will be affected by variations in ICB topography. 0.1 s of PKiKP arrival time variation corresponds to ~0.5 km of topography. Attributing the travel time residual variation to ICB topography only would lead to peak-to-peak ICB topography of 5.5 km between the large-scale regions, with 7.5 km of topography required for the small-scale scatter. Large regional variations in the radius of the inner core are probably unsustainable [*Koper and Dombrovskaya*, 2005], but small-scale topography on the ICB may be supported by the much higher viscosity of the inner core compared to the outer core [*Buffett*, 1997].

Previous studies have found much variation in the topography of the ICB. *Koper et al.* [2003] preferred CMB topography of 3.5 km to explain the observations, with negligible ICB variation. Small-amplitude ICB topography was proposed by *Cao et al.* [2007], with heights of 0.3–0.5 km varying on lateral distances of 10 km. Conversely, *Dai et al.* [2012] found that focusing is possible for two length scales of topography: height scales of 14 km varying over a distance of 6 km and heights of 4–8 km with a lateral scale of 2–4 km. Our results are in excellent agreement with these values. Thus, we suggest that small-scale topography can explain the scatter, with differences in height and length scale between regions. Focusing from small-scale topography may also be able to explain the large *PKiKP* amplitudes [*Dai et al.*, 2012].

Several mechanisms have been proposed to generate topography on the ICB. One process is convection at the top of the inner core [*Cao et al.*, 2007], which may also explain the observed hemispherical difference in seismic properties [*Wen and Niu*, 2002]. Alternatively, topography could result from rapid localized growth [*Wen*, 2006] or regional melting due to an influx of heat into the inner core [*Gubbins et al.*, 2011]. *Dai et al.* [2012] suggested that thermal or compositional variations could produce irregular topography on the boundary, which is compatible with our observations.

4.3. Implications for Inner Core Processes

Since melting and freezing of the inner core affect both *F* layer velocity properties and ICB topography, a combination of these features seems the most reasonable explanation for our amplitude ratio and travel time observations. Solidification of the inner core results in high seismic velocity in the *F* layer, while increasing ICB topography, which both produce more negative *PKiKP-PcP* travel time residuals. Conversely, melting of the inner core will generate a low-velocity *F* layer and depression of the ICB, making *PKiKP-PcP* travel time residuals more positive. These processes also result in variations in small-scale topography, which varies in magnitude and length scale between the different regions.

Small-scale variations in ICB topography would generate anomalously large *PKiKP* amplitudes [*Dai et al.*, 2012]. We also cannot rule out heterogeneities beneath the ICB and within the boundary layer affecting the *PKiKP* amplitudes [*Poupinet and Kennett*, 2004; *Koper and Dombrovskaya*, 2005; *Leyton and Koper*, 2007]. The structure in the upper 100 km of the inner core is complex and likely extends to the boundary [*Waszek and Deuss*, 2011]. If the *PKiKP* amplitudes depend on small-scale structure, whereas the primary travel time differences are due to large-scale regional variation, this will explain the lack of correlation between them.

Our observations have implications for the long-term processes of the inner core. If the inner core is laterally translating, then we expect to see strong hemispherical differences at the ICB [*Alboussiére et al.*, 2010; *Monnereau et al.*, 2010]. Hemispherical differences in the *F* layer would also be expected, assuming that the viscosity in the *F* layer is higher than that in the bulk of the outer core. However, we do not observe any hemispherical structure. Instead, our results match more closely with regional variations in growth rates

[*Aubert et al.*, 2008; *Aubert and Dumberry*, 2011; *Gubbins et al.*, 2011]. The relationship between the regional patches at the ICB and the seismic structures in the inner core currently remains unclear and requires further investigation.

5. Conclusions

The *PKiKP*/*PcP* amplitude ratios show large amounts of scatter and in many cases are much larger than can be explained by realistic density contrasts at the ICB and CMBs. This indicates that we only detect *PKiKP* signals when they are anomalously large. The theoretical difference in amplitude ratios from a hemispherical velocity structure at the ICB is much smaller than the scatter in the data, meaning that we cannot detect a hemispherical variation in amplitude ratios. Using data in which *PKiKP* is not detected above the noise level, we obtain an upper estimate of 1.2 kg m^{-3} for the density contrast at the ICB. The differential travel time residuals show scatter due to mantle structure; however, they are also correlated with the *PKiKP* residuals. This indicates that the overall variation in the residuals arises from structure in the outer core, or at the ICB. We find no evidence for hemispherical asymmetry in the residuals. Instead, we detect variation on a smaller scale. We observe distinct regional patches, which display differences in average residuals, and length scales of scatter. The large variation in the *PKiKP*/*PcP* amplitude ratios likely results from their path differences through the crust and mantle. We suggest that the differences in travel time residual may arise from large-scale velocity variations in the *F* layer, and/or small-scale topography on the ICB which varies in magnitude and length scale between region. Focusing from small-scale ICB topography can also explain the large *PKiKP*, in addition to heterogeneities in the crust. These regional differences may arise as a result of localized freezing and melting of the inner core.

Acknowledgments
L.W. is funded by a Research Fellowship from Homerton College, University of Cambridge. A.D. is funded by the European Research Council under the European Community's Seventh Framework Programme (FP7/2007-2013)/ERC grant agreement 204995, and a Philip Leverhulme Prize. We thank Vernon Cormier and an anonymous reviewer for their helpful and constructive comments. We thank Elizabeth Day and Jessica Irving for use of Mantle Mapper. The facilities of the IRIS Data Management System, and specifically the IRIS Data Management Center, were used for access to waveform and metadata required in this study. The IRIS DMS is funded through the National Science Foundation and specifically the GEO Directorate through the Instrumentation and Facilities Program of the National Science Foundation under cooperative agreement EAR-1063471 (http://www.iris.edu/wilber3/).

References

Alboussiére, T., R. Deguen, and M. Melzani (2010), Melting-induced stratification above the Earth's inner core due to convective translation, *Nature*, *466*, 744–747.
Antonangeli, D., J. Siebert, J. Badro, D. Farber, G. Fiquet, G. Morard, and F. Ryerson (2010), Composition of the Earth's inner core from high-pressure sound velocity measurements in Fe-Ni-Si alloys, *Earth Planet. Sci. Lett.*, *295*, 292–296.
Aubert, J., and M. Dumberry (2011), Steady and fluctuating inner core rotation in numerical geodynamo models, *Geophys. J. Int.*, *184*, 162–170.
Aubert, J., H. Amit, G. Hulot, and P. Olson (2008), Thermochemical flows couple the Earth's inner core growth to mantle heterogeneity, *Nature*, *454*, 758–762.
Badro, J., G. Fiquet, F. Guyot, E. Gregoryanz, F. Occelli, D. Antonangeli, and M. d'Astuto (2007), Effect of light elements on the sound velocities in solid iron: Implications for the composition of Earth's core, *Earth Planet. Sci. Lett.*, *254*, 233–238.
Buffett, B. (1997), Geodynamic estimates of the viscosity of the Earth's inner core, *Nature*, *388*, 571–573.
Bolt, B. (1972), The density distribution near the base of the mantle and near the Earth's center, *Phys. Earth Planet. Inter.*, *5*, 301–311.
Bolt, B., and A. Qamar (1970), Upper bound to the density jump at the boundary of the Earth's inner core, *Nature*, *228*, 148–150.
Cao, A., and B. Romanowicz (2004a), Constraints on density and shear velocity contrasts at the inner core boundary, *Geophys. J. Int.*, *157*, 1146–1151.
Cao, A., and B. Romanowicz (2004b), Hemispherical transition of seismic attenuation at the top of the Earth's inner core, *Earth Planet. Sci. Lett.*, *228*(3–4), 243–253.
Cao, A., Y. Masson, and B. Romanowicz (2007), Short wavelength topography on the inner-core boundary, *Proc. Natl. Acad. Sci.*, *104*, 31–35.
Chapman, C. (1976), A first motion alternative to geometrical ray theory, *Geophys. Res. Lett.*, *3*, 153–156.
Cormier, V. (1999), Anisotropy of heterogeneity scale lengths in the lower mantle from PKIKP precursors, *Geophys. J. Int.*, *136*, 373–384.
Cormier, V. (2009), A glassy lowermost outer core, *Geophys. J. Int.*, *179*, 374–380.
Dai, Z., W. Wang, and L. Wen (2012), Irregular topography at the Earth's inner core boundary, *Proc. Natl. Acad. Sci.*, *109*, 7654–7658.
Deuss, A., J. Irving, and J. Woodhouse (2010), Regional variation of inner core anisotropy from seismic normal mode observations, *Science*, *328*, 1018–1020.
Ekström, G., A. Dziewoński, N. Maternovskaya, and M. Nettles (2005), Global seismicity of 2003: Centroid-moment-tensor solutions for 1087 earthquakes, *Phys. Earth Planet. Inter.*, *148*, 327–351.
Engdahl, E., E. Flinn, and C. Romney (1970), Seismic waves reflected from the Earth's inner core, *Nature*, *228*, 852–853.
Geballe, Z., M. Lasbelis, V. Cormier, and E. Day (2013), Sharp hemisphere boundaries in a translating inner core, *Geophys. Res. Lett.*, *40*, 1719–1723, doi:10.1002/grl.50372.
Goldstein, P., D. Dodge, M. Firpo, and L. Minner (2003), SAC2000: Signal processing and analysis tools for seismologists and engineers, in *The IASPEI International Handbook of Earthquake and Engineering Seismology*, edited by W. H. K. Lee et al., pp. 1613–1614, Academic Press, London.
Gubbins, D., G. Masters, and F. Nimmo (2008), A thermochemical boundary layer at the base of Earth's outer core and independent estimate of core heat flux, *Geophys. J. Int.*, *174*, 1007–1018.
Gubbins, D., B. Sreenivasan, J. Mound, and S. Rost (2011), Melting of the Earth's inner core, *Nature*, *473*, 361–363.
Hedlin, M., and P. Shearer (2000), An analysis of large-scale variations in small-scale mantle heterogeneity using Global Seismographic Network recordings of precursors to PKP, *J. Geophys. Res.*, *105*, 13,655–13,673.
Hong, T. -K., and W. Menke (2008), Imaging laterally varying regional heterogeneities from seismic coda using a source-array analysis, *Phys. Earth Planet. Inter.*, *166*, 188–202.
Hutko, A., T. Lay, E. Garner, and J. Revenaugh (2006), Seismic detection of folded, subducted lithosphere at the core-mantle boundary, *Nature*, *441*, 333–336.
Irving, J., and A. Deuss (2011), Hemispherical structure in inner core velocity anisotropy, *J. Geophys. Res.*, *16*, B04307, doi:10.1029/2010JB007942.

Kennett, B., E. Engdahl, and R. Buland (1995), Constraints on seismic velocities in the Earth from travel times, *Geophys. J. Int.*, *122*, 108–124.
Koper, K., and M. Dombrovskaya (2005), Seismic properties of the inner core boundary from PKiKP/P amplitude ratios, *Earth Planet. Sci. Lett.*, *237*, 680–694.
Koper, K., and M. Pyle (2004), Observations of PKiKP/PcP amplitude ratios and implications for Earth structure at the boundaries of the liquid core, *J. Geophys. Res.*, *109*, B03301, doi:10.1029/2003JB002750.
Koper, K., M. Pyle, and J. Franks (2003), Constraints on aspherical core structure from PKiKP-PcP differential travel times, *J. Geophys. Res.*, *108*(B3), 2168, doi:10.1029/2002JB001995.
Krasnoshchekov, D., P. Kaazik, and V. Ovtchinnikov (2005), Seismological evidence for mosaic structure of the surface of the Earth's inner core, *Nature*, *435*, 483–487.
Leyton, F., and K. Koper (2007), Using PKiKP coda to determine inner core structure: 1. Synthesis of coda envelopes using single-scattering theories, *J. Geophys. Res.*, *112*, B05316, doi:10.1029/2006JB004369.
Li, C., R. van der Hilst, R. Engdahl, and S. Burdick (2008), A new global model for P wave speed variations in Earth's mantle, *Geochem. Geophys. Geosyst.*, *9*, Q05018, doi:10.1029/2007GC001806.
Lythgoe, K., A. Deuss, J. Rudge, and J. Neufeld (2014), Earth's inner core: Innermost inner core or hemispherical variations?, *Earth Planet. Sci. Lett.*, *385*, 181–189.
McNamara, A., E. Garnero, and S. Rost (2010), Tracking deep mantle reservoirs with ultra-low velocity zones, *Earth Planet. Sci. Lett.*, *299*, 1–9.
Miller, M., and F. Niu (2008), Bulldozing the core-mantle boundary: Localized seismic scatterers beneath the Caribbean Sea, *Phys. Earth Planet. Inter.*, *170*, 89–94.
Monnereau, M., M. Calvet, L. Margerin, and A. Souriau (2010), Lopsided growth of Earth's inner core, *Science*, *328*, 1014–1017.
Morelli, A., A. Dziewoński, and J. Woodhouse (1986), Anisotropy of the inner core inferred from PKIKP travel times, *Geophys. Res. Lett.*, *13*, 1545–1548.
Niu, F., and L. Wen (2001), Hemispherical variations in seismic velocity at the top of the Earth's inner core, *Nature*, *410*, 1081–1084.
Oreshin, S., and L. Vinnik (2004), Heterogeneity and anisotropy of seismic attenuation in the inner core, *Geophys. Res. Lett.*, *31*, L02613, doi:10.1029/2003GL018591.
Poupinet, G., and B. Kennett (2004), On the observation of high frequency PKiKP and its coda in Australia, *Phys. Earth Planet. Inter.*, *146*, 497–511.
Poupinet, G., R. Pillet, and A. Souriau (1983), Possible heterogeneity of the Earth's core deduced from PKIKP travel times, *Nature*, *305*, 204–206.
Ritsema, J., H. van Heijst, and J. Woodhouse (2004), Global transition zone tomography, *J. Geophys. Res.*, *109*, B02302, doi:10.1029/2003JB002610.
Shearer, P. (1994), Constraints on inner core anisotropy from PKP(DF) travel times, *J. Geophys. Res.*, *99*, 19647–19659.
Shearer, P., and G. Masters (1990), The density and shear velocity contract at the inner core boundary, *Geophys. J. Int.*, *102*, 491–498.
Song, X., and D. Helmberger (1998), Seismic evidence for an inner core transition zone, *Science*, *282*, 924–927.
Souriau, A., and M. Souriau (1989), Ellipticity and density at the inner core boundary from subcritical PKiKP and PcP data, *Geophys. J. Int*, *98*, 39–54.
Souriau, A. (2009), Inner core structure: Constraints from frequency dependent seismic anisotropy, *C. R. Geosci.*, *341*, 439–445.
Tanaka, S., and H. Hamaguchi (1997), Degree one heterogeneity and hemispherical variation of anisotropy in the inner core from PKP(BC) - PKP(DF) times, *J. Geophys. Res.*, *102*, 2925–2938.
Tkalĉic, H., B. Kennett, and V. Cormier (2009), On the inner-outer core density contrast from PKiKP/PcP amplitude ratios and uncertainties caused by seismic noise, *Geophys. J. Int.*, *179*, 425–443.
Tkalĉic, H., V. Cormier, B. Kennett, and K. He (2010), Steep reflections from the Earth's core reveal small-scale heterogeneity in the upper mantle, *Phys. Earth Planet. Inter.*, *178*, 80–91.
Vanacore, E., F. Niu, and Y. Ma (2010), Large angle reflection from a dipping structure recorded as a PKIKP precursor: Evidence for a low velocity zone at the core-mantle boundary beneath the Gulf of Mexico, *Earth Planet. Sci. Lett.*, *293*, 54–62.
Waszek, L., and A. Deuss (2011), Distinct layering in the hemispherical seismic velocity structure of Earth's upper inner core, *J. Geophys. Res.*, *116*, B12313, doi:10.1029/2011JB008650.
Waszek, L., and A. Deuss (2013), A low attenuation layer in the Earth's uppermost inner core, *Geophys. J. Int.*, *195*, 2005–2015.
Waszek, L., J. Irving, and A. Deuss (2011), Reconciling the hemispherical structure of Earth's inner core with its super-rotation, *Nat. Geosci.*, *4*, 264–267.
Wen, L. (2006), Localized temporal change of the Earth's inner core boundary, *Science*, *314*, 967–970.
Wen, L., and F. Niu (2002), Seismic velocity and attenuation structures in the top of the Earth's inner core, *J. Geophys. Res.*, *107*(B11), 2273, doi:10.1029/2001JB000170.
Woodhouse, J., D. Giardini, and X. Li (1986), Evidence for inner core anisotropy from free oscillations, *Geophys. Res. Lett.*, *13*, 1549–1552.
Yu, W., and L. Wen (2006), Seismic velocity and attenuation structures in the top 400 km of the Earth's inner core along equatorial paths, *J. Geophys. Res.*, *111*, B07308, doi:10.1029/2005JB003995.
Zheng, Y., and R. Wu (2008), Theory of transmission fluctuations in random media with a depth-dependent background velocity structure, *Adv. Geophys.*, *50*, 21–41.